Antihydrogen Production and Precision Spectroscopy with ATHENA/AD-1

C. Amsler[10], G. Bendiscioli[6], G. Bonomi[2], P. Bowe[1], C. Carraro[4], C. L. Cesar[7], M. Charlton[8], M.J.T. Collier[8], M. Doser[3], K. Fine[3], A. Fontana[6], M.C. Fujiwara[9], R. Funakoshi[9], J. Hangst[1], R.S. Hayano[9], H. Higaki[9], M. H. Holzscheiter[3], W. Joffrain[4], L.V. Jøergensen[8], D. Kleppner[5], V. Lagomarsino[4], R. Landua[3], D. Lindelof[10], E. Lodi-Rizzini[2], M. Macri[4], D. Manuzio[4], G. Manuzio[4], M. Marchesotti[6], P. Montagna[6], H. Pruys[10], C. Regenfus[10], P. Riedler[10], A. Rotondi[6], G. Rouleau[3], G. Testera[4], T.L. Watson[8], D.P. van der Werf[8], T. Yamazaki[9], and Y. Yamazaki[9]

[1] Inst. for Physics & Astronomy, University of Aarhus, DK-8000 Aarhus C, Denmark
[2] Brescia University & INFN, Brescia, Italy
[3] CERN, CH-1211 Geneva 23, Switzerland
[4] Genoa University & INFN, Via Dodecaneso 33, I-16146 Genoa, Italy
[5] AMO Institute, MIT, Cambridge, MA, United States
[6] Pavia University & INFN, Pavia, Italy
[7] Fed. Univ. Rio de Janeiro (UFRJ), BR-21945 Rio de Janeiro, Brasil
[8] University of Wales Swansea, Wales, United Kingdom
[9] Inst. of Physics and Department of Physics, Tokyo University, Tokyo, Japan
[10] Physik Institut, Zürich University, Winterthurerstrasse 190, CH-8057 Zürich, Switzerland

Abstract. CPT invariance is a fundamental property of quantum field theories in flat space-time. Principal consequences include the predictions that particles and their antiparticles have equal masses and lifetimes, and equal and opposite electric charges and magnetic moments. It also follows that the fine structure, hyperfine structure, and Lamb shifts of matter and antimatter bound systems should be identical.

It is proposed to generate new stringent tests of CPT using precision spectroscopy on antihydrogen atoms. An experiment to produce antihydrogen at rest has been approved for running at the Antiproton Decelerator (AD) at CERN. We describe the fundamental features of this experiment and the experimental approach to the first phase of the program, the formation and identification of low energy antihydrogen.

1 Motivation for Experiments with Low Energy Neutral Antimatter

CPT invariance is a fundamental property of quantum field theories in flat space-time which results from the basic requirements of locality, Lorentz invariance and unitarity [1,2,3,4,5]. A number of experiments have tested some of these predictions with impressive accuracy [6], e.g. with a precision of 10^{-12} for the difference between the moduli of the magnetic moment of the positron and the electron [7] and of 10^{-9} for the difference between the proton and antiproton charge-to-mass ratio [8].

However, the most stringent CPT test comes from a mass comparison of the neutral kaon and antikaon, where the tremendous accuracy of 10^{-18} has been reached, albeit in a theoretically dependent manner. Not only does the comparison only restrict CPT violation to 1 part in 10^3 of CP violation, the origin of which itself is not fully understood, but it has been argued [9] that the analysis leading to this limit assumes the validity of the standard model, which in itself does not contain a mechanism for CPT violation.

Hydrogen has been an extremely important tool in the development of quantum mechanics and quantum electrodynamics (QED). Spectroscopy on hydrogen has reached "astronomical" precisions and has thereby helped to establish QED as the most successful physical theory to date. There are a number of reasons to expect that antihydrogen will play an equally important role in the development of modern physics. Firstly, using the same experimental methods as developed for hydrogen spectroscopy, high precision comparison of the two systems may be achieved. Since such comparative measurements do not require knowledge of the absolute frequency the need for ultra-precise frequency standards is alleviated, thus paving the way towards yet higher accuracies. Secondly, since antihydrogen is a mostly electromagnetic system (weak interaction, or parity violating, effects are small and the same for hydrogen and antihydrogen) the interpretation of any deviation between hydrogen and antihydrogen is less model dependent than in the case of the kaon mass difference.

One of the cornerstones of gravity theories is the weak equivalence principle (WEP), which requires the gravitational acceleration of a falling object to be independent of its composition. The gravitational acceleration of a variety of composite objects of ordinary matter have been shown to be equal with a precision of 1 part in 10^{12} in the Eötvös-Dicke experiments [10]. Arguments against "antigravity", or more generally speaking against a difference in gravitational acceleration of matter and antimatter, have been given by numerous authors and have been discussed and summarized in detail by Nieto and Goldman [11]. On the other hand, very few observations, and certainly no quantitative measurements, exist for the gravitational acceleration of elementary particles, aside from the experiments by W. Fairbank and F. Witteborn [12] on free electrons and the neutron interferometric measurements by Overhauser and coworkers [13]. And there has yet to be an experimental test of the WEP for an elementary particle and its antiparticle, such as the antiproton and proton.

Antihydrogen, since it is a stable and neutral antimatter object, would allow direct tests of the gravitational interaction of antimatter with the gravitational field of the Earth free from the problems associated with electromagnetic interactions which burden such investigations with charged particles. Whilst low energy antihydrogen would clearly avoid the problems of electrical stray fields, direct (ballistic) measurements of the gravitational acceleration will be by no means trivial. The largest problem to be faced will be the low expected number of atoms produced and the concomitant poor statistics of any free fall measurement. Furthermore it must be noted that the kinetic energy of antihydrogen cooled to the photon recoil limit of 3.2 mK (assuming standard Doppler cooling

of antihydrogen in the ground state can be accomplished) is still very high on the scale of gravity. A cloud at this temperature will exhibit a vertical spread in the gravitational potential of the Earth of 2.6 meter. Conversely, the velocity spread in such a cloud would be around 7 ms^{-1}, which would cause it to spread significantly faster than it would fall under the influence of gravity.

In the absence of a direct measurement on antiprotons and protons one can use various indirect arguments to study the compliance of antiparticles with the WEP. In this context it is important to note that if the antiproton or the positron violate the WEP, this would not imply a violation of energy conservation [14] or of CPT symmetry [15].

A manifestation of gravity can be found in the red shift of "clock" frequencies in a gravitational field. Relativistic effects proportional to the gravitational potential arise since a fraction of the binding energy consists of the gravitational potential energy [16]. The usual gravitational red-shift is then simply the consequence of the assumption of the validity of the WEP for the gravitational field [17,18,19]. Conversely, the red-shift of clock frequencies may be formulated as a test of the WEP for the energy content of clocks [20]. Therefore, a measurement of the transition frequencies in a clock based on antimatter, and the comparison with its matter counterpart, would constitute a test of the WEP which is complementary to a direct measurement of the gravitational acceleration.

2 Antihydrogen Formation

To effectively form a bound antiproton-positron state starting from free particles, excess energy and momentum has to be carried away by a third particle. Various schemes for producing antihydrogen have been proposed and discussed in some detail [21,22,23,24,25,26,27], with the first mention of the possible production of antihydrogen in traps by Dehmelt and co-workers [28].

In principle, the simplest process is spontaneous radiative recombination (SRR):

$$e^+ + \overline{p} \rightarrow \overline{H} + h\nu. \tag{1}$$

The rate for this process can be increased by laser stimulation [22]:

$$e^+ + \overline{p} + k\,h\nu \rightarrow \overline{H} + (k+1)\,h\nu. \tag{2}$$

A different approach to enhance the rate of antihydrogen formation is based on three-body recombination (TBR) [21]:

$$e^+ + e^+ + \overline{p} \rightarrow \overline{H} + e^+ \ . \tag{3}$$

The above reactions require that two plasmas of opposite charge (antiprotons and positrons) are trapped and brought into contact. Alternatively, recombination by crossing a beam of positronium (either in the ground state or in low-lying excited states) with antiprotons has been proposed (see references [23,24,25,26]):

$$Ps + \overline{p} \rightarrow \overline{H} + e^- \ , \tag{4}$$

and

$$Ps^* + \overline{p} \rightarrow \overline{H^*} + e^- \ , \tag{5}$$

Following the discovery of metastable bound states of antiprotons in helium gas [29] the use of this product as an intermediate step towards antihydrogen formation has been discussed :

$$e^+ + \alpha\overline{p}e^- \Rightarrow \overline{H} + \alpha + e^-, \tag{6}$$

Unfortunately the formation of antihydrogen with this method must occur in a dense target and the expected lifetime of the produced antihydrogen is extremely short [30].

Since the ultimate goal consists of high precision spectroscopy on (trapped) antihydrogen, the main focus of future experiments must be on the production and storage of antihydrogen atoms at very low energies. Thus, the recombination technique used should have the prospect to:

- provide sufficient numbers of antihydrogen atoms to allow the use of standard spectroscopic methods,
- produce the atoms at very low temperatures (T $\leq$ 1 K) to allow trapping within achievable magnetic well depths,
- form antihydrogen atoms in the ground state or in excited states, and
- achieve the above within a time period short compared to the storage time of the charged plasmas.

Currently only reactions (1) - (3) are considered serious contenders for achieving the goal of precision spectroscopy of cold antihydrogen atoms. Spontaneous radiative recombination (reaction 2) was first suggested as a source of antihydrogen by Budker and Skrinsky [31] and involves a photon carrying away the binding energy plus the kinetic energy of the positron in the antiatomic center of mass frame. The matter equivalent of this reaction has been studied for many years [32] and has received interest in recent years since recombination between ions and electrons is a significant loss mechanism in storage rings with electron cooling. For this reason a wealth of theoretical and experimental data exists for this reaction in co-moving beams. The recombination process does not depend on the average longitudinal energy but only on the relative longitudinal and transverse velocity distributions (or equivalent temperature) of the two plasmas in the moving frame. Since the typical temperatures of trapped clouds and those of co-moving beams are similar, the storage ring results can be used to estimate the corresponding recombination rates in traps.

The cross sections, σ_n^{SRR}, for radiative capture to a state of principal quantum number n have been given in analytic form [32] as

$$\sigma_n^{SRR} = 2^5 \frac{\pi\alpha^3}{3\sqrt{3}} a_o^2 E_o/nE_e(1 + n^2 E_e/E_o) \tag{7}$$

Here α is the fine structure constant and a_o is the Bohr radius. This expression is valid for the case when the kinetic energy, E_e, of the positrons (electrons) in

the rest frame of the antiprotons (protons) is much less than the binding energy, E_o, of the lowest atomic bound state. This cross section decreases at high n, and the total capture cross section, σ^{SRR}, can be obtained by summing over all n up to some "cut-off" level at which the nascent atoms are field ionized, either by collisions or by external electric fields. (For example, an antihydrogen atom in an n=200 state is ionized by an electric field of around 1 Vcm^{-1} or by a collision with 0.34 meV kinetic energy. Typical values of σ^{SRR} range from 5x10^{-21} to 10^{-16} cm^2 for values of E_e~1 eV - 0.1 meV.)

The recombination coefficient α^{SRR} is obtained by integrating over the product of the cross section and the distribution of relative velocities between the antiprotons and positrons, normally taken as v_e ($E_e = mv_e^2/2$), assuming the heavier antiproton to be at rest. To get a feel for the size of α^{SRR} we assume the relative velocity can be described by a fixed value for the positron kinetic energy and obtain:

$$\alpha^{SRR} = \langle \sigma^{SRR}(v)v \rangle = \begin{cases} 3.2 \cdot 10^{-13} & cm^3 s^{-1} \quad (1 \text{ eV}) \\ 7.1 \cdot 10^{-12} & cm^3 s^{-1} \quad (10 \text{ meV}) \\ 0.9 \cdot 10^{-10} & cm^3 s^{-1} \quad (0.1 \text{ meV}) \ . \end{cases} \tag{8}$$

These values agree within a factor two or better with more elaborate calculations [33] as well as with experiments at the Test Storage Ring in Heidelberg [34]. A more general discussion of these calculations, as applicable to antihydrogen formation, has been given by Müller and Wolf [35].

The spontaneous recombination rate can be enhanced by stimulating the free-bound transition by a laser (CW or pulsed) tuned to the resonance energy for a transition from the continuum to a specific, low lying n level (i.e. a CO_2 laser can be used to enhance the population of the $n = 11$ state) [36].

If the density of positrons is increased, the likelihood to have a second positron close by during a collision between an antiproton and the first positron increases. In this case the second positron can carry away the excess energy and momentum and a bound state of antihydrogen can be formed. This three-body recombination reaction (TBR) is, as described below, thought to be extremely efficient if the positron plasma is dense and cold. The use of this reaction for antihydrogen formation was first suggested by Gabrielse *et al.* [21]. The antihydrogen production rate (which corresponds to the recombination rate in conventional plasma physics) can be written as

$$R_{\bar{H}} = 6 \times 10^{-12} \left(\frac{4.2}{T} \right)^{9/2} n_{e^+}^2 . \tag{9}$$

This formula for the rate per trapped antiproton per second is notable for its very strong, T$^{-9/2}$ (in degrees K), positron temperature dependence and the presence of the positron density, n_{e^+} (in cm^{-3}), to the second power. In their analysis Gabrielse *et al.* [21] assumed that a plasma of 10^7 e$^+$ cm^{-3} would be produced at 4.2 K which yields a production rate of $R_{\bar{H}}$~ 600 s^{-1}. Glinsky and O'Neil [37] have re-examined this problem from a plasma physics viewpoint. They find that the combination rate given by equation (9), which is actually that pertaining to

zero magnetic field, is reduced by an order of magnitude in a highly magnetised plasma of the type likely to exist in a Penning trap. In essence, this is caused by the constraint imposed on the positron orbits, since in the absence of collisions they cannot cross the field lines.

An alternative approach to the (zero magnetic field) three-body reaction has been discussed by Pajeck and Schuch [38] who noted that recombination rates for reaction (3) can be related to the time-reversed process (using charge conjugation and time reversal) of electron impact ionization of Rydberg atomic hydrogen atoms. Using this relationship, the three-body recombination coefficient α_n^{TBR} for capture into a state n has been found to be

$$\alpha_n^{TBR} \approx 64\pi^2 \alpha c a_o^5 \left(\frac{13.6eV}{kT_e}\right) n^6 \ . \tag{10}$$

This expression reveals the steep n-dependence of this process, showing that very high Rydberg states are favored.

3 The ATHENA Project

Two experiments approved for running at the Antiproton Decelerator (AD) at CERN have made the production and precision spectroscopy of antihydrogen their primary goal. Here we describe in detail the experimental approach and first results from the ATHENA collaboration. The name ATHENA stands for **A**ppara**T**us for **H**igh Precision **E**xperiments with **N**eutral **A**ntimatter (or **A**n**T**i**H**ydrog**EN** **A**pparatus for short). The main features of the ATHENA approach consists of using the highest density plasmas of both positrons and antiprotons in order to obtain a high antihydrogen production rate relying on spontaneous radiative recombination alone.

To minimize interference between the different plasma collection schemes used it was decided to use a spatially separated system. The antiproton collection, cooling, and compression is housed in the same superconducting magnet system as the recombination trap, but the positron accumulator is a stand-alone system connected to the main apparatus by a beam line incorporating differential pumping and a fast valve. Figure 1 shows a schematic lay-out of the apparatus and the following sub-sections describe the individual parts of the apparatus in more detail.

Using the method developed in experiment PS200 at LEAR [39], antiprotons are captured in an approximately 30 cm long, cylindrical Penning-Malmberg trap, and cooled to thermal equilibrium with the ambient temperature of the surrounding apparatus by electron cooling. Assuming 5 $\times 10^7$ antiprotons per pulse from the AD and a 1 % capture efficiency [40] about 20 pulses would be needed to achieve the goal of collecting 1 $\times 10^7$ antiprotons. Allowing 3 minutes between pulses for electron cooling this process will take about one hour.

For the accumulation of the positron plasma we plan to use a system based upon the positron accumulator presently operated at the University of California in San Diego, in which 10^8 low energy positrons are routinely accumulated in

a few minutes. Once the positrons have been accumulated in this set-up they can be transferred to the main system in preparation of recombination with antiprotons.

Once an antiproton and positron have combined, electrical confinement forces cease and the antihydrogen atom will escape, hit an electrode, and annihilate. During the early stages of the experiment no attempt will be made to trap the produced antihydrogen and the annihilation signature will be one of the most important diagnostics tools.

The detectors necessary to study the formation and subsequent annihilation of antihydrogen as a function of time after merging of positrons and antiprotons and as a function of various experimental parameters (well depths of antiproton/positron traps, density of charged particle clouds, etc.) will be mounted around the recombination trap in the space between the inner vacuum shell and the main magnet coils. This configuration minimizes multiple scattering of the annihilation products on their way from the trap to the detector and is necessary to achieve the high spatial resolution in vertex reconstruction which is desirable at least during the early stages of the experiment for proper identification of antihydrogen and for better back ground rejection.

For future confinement of the produced antihydrogen atoms the interaction between the magnetic moment of the atoms and a magnetic field gradient can be used. This will require superimposing a strong magnetic field gradient onto the constant field necessary for the Penning trap. Typically a combination of quadrupole coils (Ioffe bars) for radial confinement and Helmholtz coils for the axial confinement is used [41]. Such a system would interfere with the current design of the annihilation detector and also may effect the confinement properties

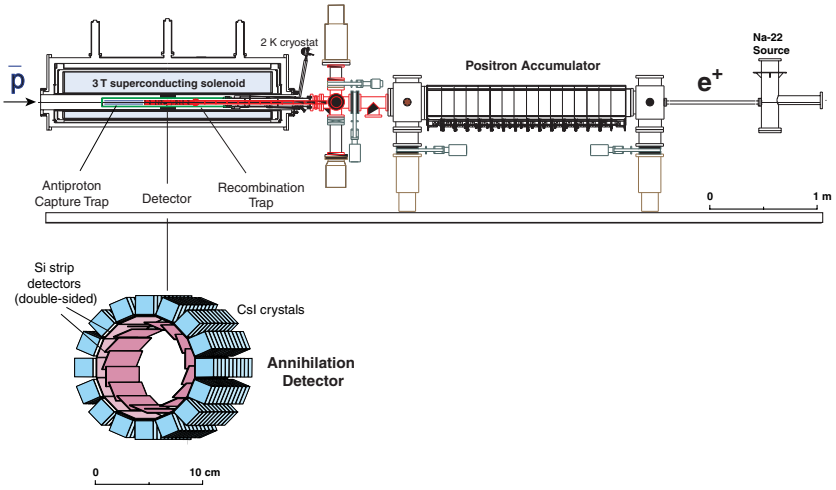

Fig. 1. General lay-out of ATHENA experiment. Shown are the positron accumulator and the main magnet system holding the antiproton catching trap, the recombination trap, and the annihilation detector surrounding the recombination region

of the charged particle plasmas. For this reason the project has been separated in phase I - formation - and phase II - precision spectroscopy - of antihydrogen.

3.1 The Charged Particle Traps in ATHENA

The geometry of the ATHENA capture and cooling trap is similar to that used by PS200. It is housed in the original superconducting magnet system of experiment PS200, a large bore solenoid with a homogeneous magnetic field (ΔB/B $\leq 10^{-4}$) of about 3 Tesla over a one meter long section. This magnet system has been modified to adapt to the requirements of the ATHENA experiment. The trap structure itself is contained within a separate vacuum enclosure, which also accommodates the recombination trap and the internal positron storage trap. This enclosure is completely separated from the magnet isolation vacuum and can be cooled to about 2 K using a continuous flow cryostat. Owing to the very good vacuum (p $\leq 10^{-13}$ Torr) which can be reached with such a cryogenic system [42], it is expected that the background from random annihilation of antiprotons and positrons by collisions with the residual gas is much smaller than the signal from antihydrogen annihilation on the trap walls. This background can be further reduced by requiring spatial and temporal coincidences between antiproton and positron events.

A gas switch consisting of an additional space between the nitrogen bore and the inner region of the magnet bore has been added. By evacuating this region, the nitrogen dewar becomes separated from any radiated heat originating from the magnet bore, allowing access to the detector without disturbing the cryogenics of the magnet.

The antiproton capture trap consists of 10 cylindrical electrodes made of gold-plated aluminum, with radius r = 1.25 cm and various lengths, as shown in figure 2. This trap structure includes seven electrodes (Ring, CMP1L, CMP2L, CMP3LA, CMP1R, CMP2R, CMP3RA) used to create a harmonic field region as in a Penning trap (the ring is split in four sectors for plasma compression), a few electrodes on the left and right of the harmonic region (CMP3LB, CMP3RB,CMP3RC) used to shape the electric field during various phases of particle transfer and handling, and the two extreme electrodes (labelled as HVL and HVR) for applying the high voltage necessary to capture antiprotons. The antiproton entrance electrode (HVL) incorporates the final antiproton degrader foil.

Around the trap two resonant circuits are mounted to detect and drive the electron and antiproton axial motion. The cables for routing the signals and the bias voltage back and forth to the cold nose are encapsulated inside a thin stainless steel tube. This tube can be evacuated independently from the rest of the system to prevent outgasing from these cables to deteriorate the cryogenic vacuum. The electrons for cooling the antiprotons are loaded into the harmonic region of the capture trap from an electron source (a filament) placed in the positron transfer region which is mounted on a movable support. Non-destructive diagnostics allows the measurement of particle numbers by driving a coherent motion of the particle cloud by an RF burst and then measuring the (decaying)

amplitude of the induced signal in the electrodes. It has also been shown that it is possible to temporarily remove the electron cloud from the central region to measure the characteristics of the antiproton cloud separately.

The recombination trap structure consists of 19 cylindrical electrodes with a radius of 1.25 cm and a total length of 40.6 cm. It serves several purposes: (1) the capture, cooling and compression of positrons after transfer from the positron accumulator, (2) the storage of antiprotons transferred from the capture trap, and (3) the injection of antiprotons into the positron plasma. The trap electronics consists of tuned circuits for non-destructive diagnostic, fast high voltage (≤ 100 V) pulsers allowing the manipulation of the two plasmas, and wave form generators suitable for the compression and the alignment of the particle clouds. We currently envision recombination by sending antiprotons with energies below 1 eV through a dense positron plasma (10^8 e^+/cm^3) of 5-10 cm length. Under these conditions, antiprotons experience an energy loss of about 100 meV/cm due to their Coulomb interaction, thus decelerating and eventually diffusing through the plasma. Based on the cross-section for spontaneous radiative recombination alone, an antihydrogen formation rate of about 20 sec^{-1} has been estimated. If antiprotons exiting the plasma can be collected and re-sent into the positron cloud, this rate will go up by a corresponding factor. Due to the highly modular design, other options, like recycling the antiproton cloud through a shorter positron plasma, or overlapping the plasmas in a nested trap configuration are also accessible with this set-up.

3.2 First Capture of Antiprotons in the ATHENA Catching Trap

The ATHENA high voltage switching system allows the capture of antiprotons if their kinetic energy is less than 15 keV. Since the initial kinetic energy before degradation is 5.3 MeV, the amount and the geometry of the various materials in the beam trajectory (position monitors, windows, degrader, entrance electrode) must be optimized to obtain the greatest possible fraction of antiprotons at low energy. Previous studies [40] have shown that this is achieved when the degrading material is chosen to transmit just half of the incoming beam, with the

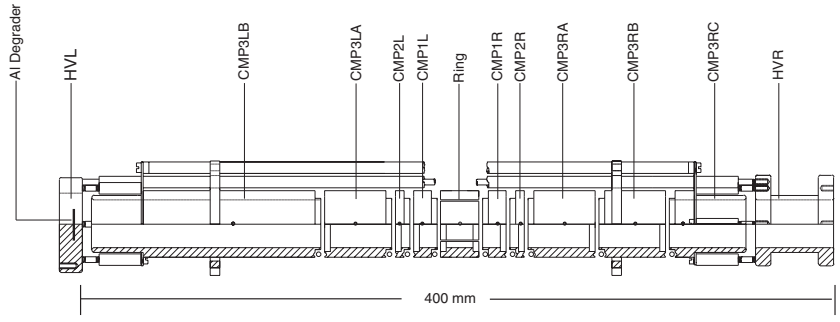

Fig. 2. Electrode structure of the ATHENA catching trap

remaining particles annihilating in the degrader. We have used two independent program packages, SRIM2000 (a successor of the original TRIM code) [43] and GEANT3.0 [44], to simulate our experimental set-up [45]. Both codes use Monte Carlo routines to model the energy loss of particles in matter, with GEANT additionally being capable to generate trajectories of the particles outside the material, including effects of external electric and magnetic fields. Both codes rely on empirical data for cross sections of the different energy loss processes considered, which turns out to be a weakness especially at the lower energies of interest for trapping where such data are not readily available. Nevertheless, reliable results can be obtained by carefully monitoring the input characteristics and correcting for the known systematic uncertainties at lower energy.

At the AD, an antiproton pulse is sent to the ATHENA experiment at a momentum of 100 MeV/c, equivalent to a kinetic energy of 5.3 MeV. These particles traverse an initial rotatable aluminum foil for fine adjustment of the degrading stack, a 67 μm Silicon beam monitor, a 25 μm stainless steel vacuum isolation window, and the final degrader foil consisting of 70 μm aluminum, which serves also as the high voltage entrance electrode of the capture trap. Both GEANT and SRIM were used to calculate the optimum thickness of the final degrader foil. Results obtained for the optimum thickness of the rotatable foil for the two codes were 40 μm and 65 μm respectively. The difference between the two codes may most likely be attributed to the difference in the data sets for the energy loss cross sections used by the programs. SRIM does not contain any information about the difference in stopping power for antiprotons vs. protons, the so-called Barkas effect [46]. Antiprotons appear to have a higher effective energy than protons, which was taken into account in our calculations by increasing the input value for the kinetic energy of the antiprotons from 5.3 MeV to 5.5 MeV, following results obtained by the PS196 collaboration at LEAR [47]. The version of GEANT used for our calculations has been extended to low energies (= 50 keV) to take into account measured antiproton cross sections on Al, Si, and other relevant materials, and no energy correction was applied in this case.

In addition we performed a test experiment using a stack of 6 Si diodes of 6 μm thickness. A test beam from the AD was degraded in an Al foil to stop in the Si diode stack before traversing all 6 diodes. Indeed, antiproton correlated signals were observed except for the last two diodes, which showed a much lower signal. These signals were consistent with a five times lower energy deposit due to minimum ionizing pions from annihilation. Results of these tests were in good agreement with the simulations mentioned above, but still left an overall uncertainty of 10 - 20 μm.

To allow for the systematic shift between the different results we performed the initial test runs with the final degrading foil thickness of 70 μm and added a rotatable foil before the silicon detector, allowing a continuous variation of the total degrader thickness over the range of interest. In figure 3 the results of the first test runs are shown, giving the total thickness of aluminum needed for optimum degrading as 114 μm (the sum of the 70 μm degrader foil and the thickness of the rotatable foil at peak efficiency). This result agrees slightly better

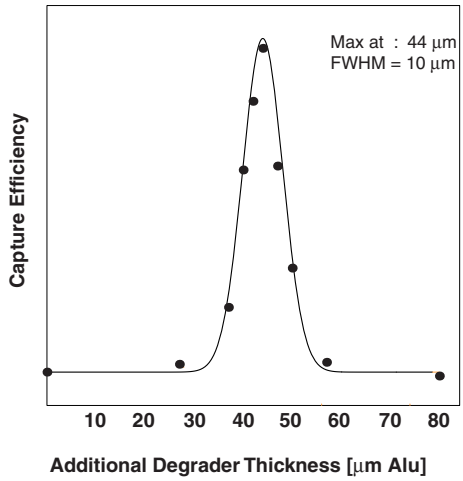

Fig. 3. Number of antiprotons trapped vs. thickness of additional degrader material in the particle path

with the estimate from SRIM, indicating a possible mismatch of the GEANT input data set for ultra-low energies.

Using the optimum setting for the degrading stack obtained from these tests we were able to capture up to 10,000 antiprotons from a single shot from the AD. These antiprotons were then cooled using electrons pre-loaded in the harmonic region of the capture trap. Figure 4 shows the antiproton annihilation signal obtained by releasing first any antiprotons remaining in the HV well of the capture trap and then with a short delay, opening the inner, harmonic, low voltage well of the trap. Increasing the interaction time between antiprotons and electrons by increasing the time delay between capture and release the signal resulting from opening the small trap was getting stronger and a large fraction of the captured antiprotons had been cooled to eV energies after 20 seconds. This allowed us now to re-open the HV switch of the capture trap before the next AD pulse would arrive to add more antiprotons to the small, central trap region. This stacking was successfully demonstrated for about 10 successive AD pulses during these test runs.

3.3 The ATHENA Positron Accumulator

Since antihydrogen formation rates increase at least linearly with the positron density, it is advantageous to use of a copious source of cold positrons. We have chosen a design based on a scheme developed by C. Surko et al. at the University of California at San Diego [48]. This type of positron accumulator supplies (depending on the strength of the radioactive source) 10^7-10^8 positrons with a repetition time of few minutes, well adapted to the AD cycle.

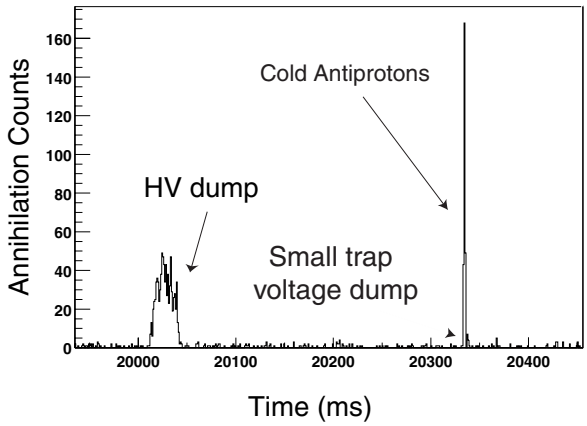

Fig. 4. First demonstration of electron cooling in the ATHENA test runs. The peak on the right side is produced by antiprotons which have been cooled to energies below 10 eV and trapped in the central, harmonic region of the ATHENA catching trap

The scheme is based on a nitrogen buffer gas for moderation and trapping of a continuous beam of positrons, which emanates from an encapsulated 9 mCi ^{22}Na β^+ radioactive source. The source is mounted on a cryogenic cold-head. A solid neon moderator, grown directly on top of the source at T= 5.5 K, slows the positrons down to epi-thermal energies of a few eV, which are then guided into the trapping region by using an axial magnetic guiding field of 250-300 Gauss. A kink of 2 cm in the positron path removes the source from the direct line of sight with the remainder of the apparatus. The source-moderator configuration has been extensively tested and regularly delivers about 10^6 moderated positrons per second with an energy spread of about 2.5 eV [49].

The electrode array of the main trapping region consists of a set of eight separate gold-plated aluminum electrodes. With the appropriate bias applied, the positrons are confined in axial direction after the initial trapping, and a 0.15 T axial magnetic field supplies the radial confinement. The physical dimensions of the electrodes (Fig. 5) allow a pressure gradient to develop along their length. Nitrogen gas flows in midway along electrode II and is pumped out at either end or through a set of three vents located at the end of the same electrode. The positrons are trapped and cooled within the electrode array through collisions with the buffer gas atoms. The nitrogen gas pressure is tuned such that on average a positron entering from the source region will experience one inelastic collision with a nitrogen molecule during one pass through the system. Now confined and unable to escape, subsequent collisions will finally confine the positron to electrodes V and VI in less than a second.

The exact electric potentials and potential steps applied to the electrodes are crucial to maximize the number of trapped positrons eventually confined in

the last stage. The gas pressure here is much lower, reducing annihilation losses yet cooling the positrons to room temperature in less than 1 second, by either exciting nitrogen molecules or by direct momentum transfer. The accumulation cycle continues until an equilibrium state is reached between positron trapping and losses due to annihilations and plasma expansion. The goal is to reach an equilibrium at about 10^8 positrons. The buffer gas supply is then switched off and the buffer gas is pumped out using high performance cryopumps, reaching a pressure of approximately 10^{-10} mbar in about 20 seconds, corresponding to a positron life time of about 1 hour.

The transfer section between the positron accumulator and the recombination trap region is a crucial component of the experiment. It must retain the vacuum integrity of the UHV region of the recombination section while permitting a high efficiency transfer of positrons. The two vacuum systems are separated by a valve - situated on the downstream side and only opened for about 1 sec during the transfer - and a thin cylindrical tube (r=1 cm, l = 10 cm) yielding a low conductance (7 liters/sec). An extra solenoid surrounds the tube to avoid the deflecting effect of magnetic stray fields between the two magnetic fields. During a positron transfer, the solenoid produces a 1 Tesla magnetic field for about 1 sec, thus reducing diameter of the positron beam to be lower than that of the low conductance tube. A differential pumping port is located at the center of the solenoid to maintain the pressure difference between the positron section and the recombination section. Two movable radial profilers monitor the alignment of the positron beam. The first profiler is mounted after the positron trap, while the second one is located just before entering the high magnetic field of the recombination magnet.

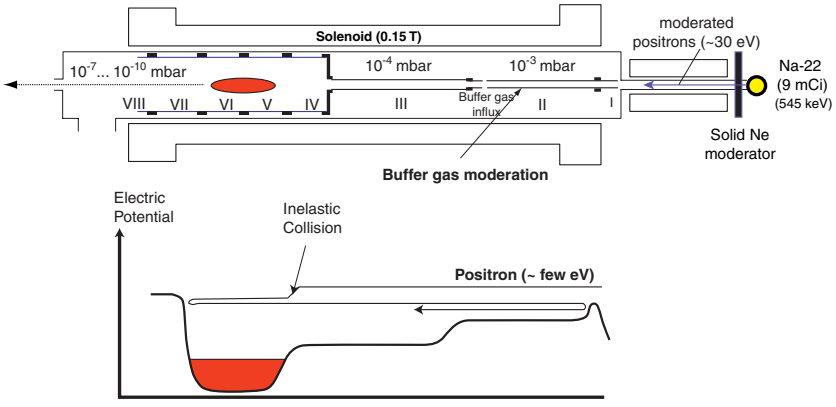

Fig. 5. The ATHENA positron accumulator. Positrons entering from the right are slowed down by collisions with the buffer gas in a single passage through electrodes I - VIII and thereby captured in the trap

3.4 Antihydrogen Detection

The purpose of the detector surrounding the antihydrogen trap is to discriminate between signals due to the annihilation of antihydrogen and those due to the trapped clouds of antiprotons and positrons. For this, one needs to provide temporal and spatial coincident detection of the annihilation of an antiproton and a positron. It should also allow reconstruction of the annihilation vertex with sufficient resolution to discriminate between annihilations on the wall of the charged particle traps and those resulting from possible collisions with residual gas atoms. In addition it must have a sufficiently high rate capability to allow the study of the time evolution of the recombination process.

The antihydrogen detector for ATHENA consists of two parts: (i) the detection of charged particles stemming from the annihilation of an antiproton with matter in or around the recombination trap, and (ii) the detection of the two back-to-back 511 keV γ-rays from positron-electron annihilation. For the best detection efficiency, the detector must be positioned as close as possible to the recombination trap, and cover as large as possible a solid angle. This, together with the calculated energy loss and scattering in the material of a typical superconducting magnet coil, leads to the requirement that the detector be placed inside the superconducting solenoid. In order to use commercially available detector and electronics components, the detector should be held at liquid nitrogen temperature or above to assure that both types of detectors, as well as the read-out electronics to be used, will work with the required performance [50].

The lay-out of the detector is shown in Fig. 6. Two layers of 16 silicon strip detector modules each for charged particle tracking and vertex reconstruction are surrounded by a cylinder constructed of 16 rows of 12 CsI (pure) crystals for the detection of the two 511 keV γ-rays. This arrangement gives a large solid angle coverage for both particle types and a sufficiently fine resolution for vertex reconstruction.

Charged Particle Detection

Antiproton-matter annihilation at rest produces on average 3 charged pions with momenta around 300 MeV/c. These particles must first traverse the trap electrodes, the wall of the surrounding vacuum vessel, the walls of the inner dewar, and finally the walls of the enclosure of the detectors. Multiple scattering in these layers leads to an uncertainty of the annihilation vertex position of about 0.5 mm and the accuracy of the hit measurement in each of the two layers of the silicon strip detector should be matched to this extrapolation accuracy.

The two layers of charged particle detectors each consist of sixteen double-sided silicon microstrip detector modules 162 mm long, 19 mm wide, and 380 μm thick. These are constructed from two 81 mm long double sided detectors (n-bulk), produced by SINTEF, Norway. Each detector has 128 p^+ readout strips with two floating intermediate strips (for the measurement of Φ) and 128 n^+ pads on the opposite side (for the measurement of z). The floating intermediate strips

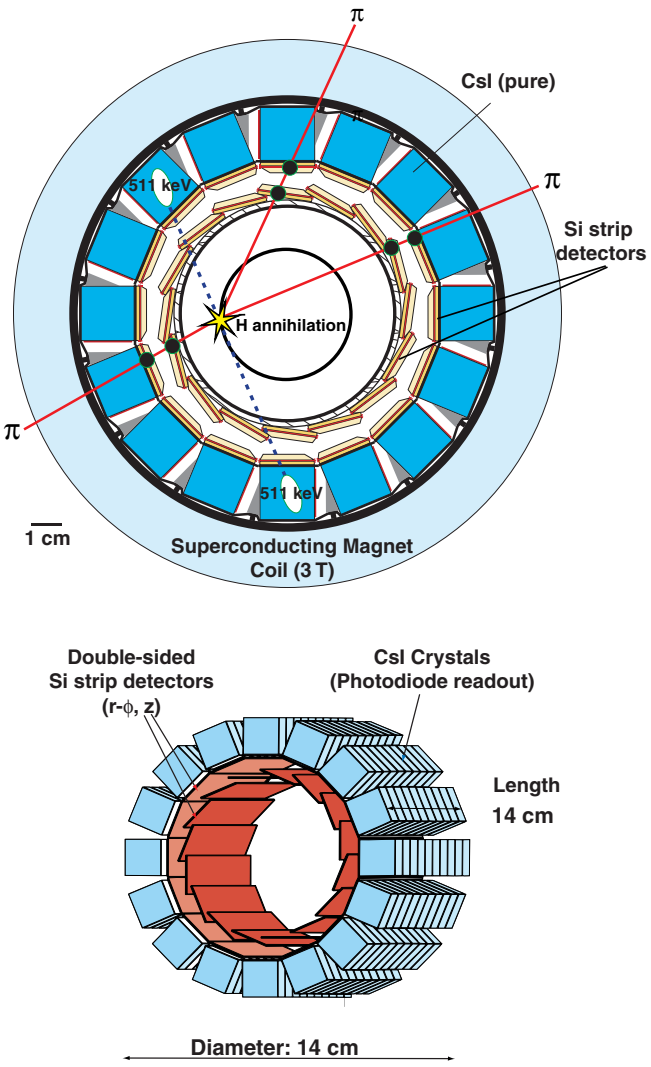

Fig. 6. Cross sectional view of the annihilation detector showing the inner two layers of silicon strip detectors for charged particle detection and the outer cylinder of CsI crystals for 511 keV γ detection

provide an improved position resolution on the p^+ side by capacitive coupling. The two layers are separated in the radial direction by 6 mm to give the necessary angular resolution.

The 2 x 128 channels from each detector are connected to two self-triggering VA2-TA amplifiers developed in collaboration with IDE AS (Norway). The 256 channels are readout sequentially with a frequency of 5 MHz and are fed

through a repeater card to ADC's (CAEN modules). The hybrids carrying the VA2-TA chips, their associated electronics, and the repeater card were designed within the collaboration.

511 keV γ-ray Detection

The γ-ray detector is a cylindrical electromagnetic calorimeter 14 cm in length consisting of 16 rows of 12 crystals of pure CsI, each 17 $\times$17 $\times$ 13 mm^3 in size, and individually wrapped in Teflon.

To understand the scintillation behavior of crystals at low temperatures we performed some systematic R&D. A cryogenic test bench was built for measuring the light output and decay time of various crystals. Measuring the relative pulse height from a monochromatic γ-source as a function of temperature we found the light output for pure CsI to increase by a factor of about 5 when cooled from room temperature down to 117 K, making it possible to detect the low energy 511 keV photons with good energy resolution. At the same time the mean decay time increases to about 1 μs, but this is still sufficiently fast for the detection of positron annihilation in ATHENA. Each crystal is read out by a segmented photo diode, thus reducing capacitive coupling and electronic noise, using the VA2-TA amplifiers. Since the maximum light emission in pure CsI at 77 K occurs at 345 nm the photodiodes had to be manufactured without protective windows and with a n^+ implantation depth of as little as 150 nm to allow blue light to reach the depletion zone.

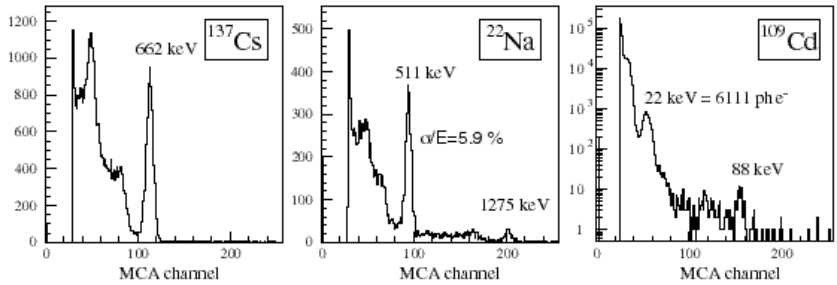

Fig. 7. Energy spectrum of 662 keV photons detected in CsI at 77 K from the ^{137}Cs β^- emitter (left) showing the photo peak and the Compton plateau. The low energy peak is due to photons back-scattered from the container. A similar spectrum is obtained for 1275 keV photons from the ^{22}Na β^+ emitter (middle). In this case one also observes the 511 keV line from positron annihilation and its corresponding Compton plateau. The resolution is better than 6 % at 511 keV. The right spectrum shows the response of the photodiode to 22 and 88 keV X-rays from ^{109}Cd. A CsI light yield of 26,000 photons/MeV at 511 keV is derived from this spectrum, assuming about 6000 electron-hole pairs for 22 keV X-rays. This is however a lower limit, as it assumes 100 % quantum efficiency for the photodiode

Figure 7 shows the photon spectrum from ^{137}Cs and ^{22}Na sources. They were obtained with a 1 cm^3 pure CsI crystal at 117 K coupled to the photodiode with optical silicon grease. The light output was 26,000 photons/MeV, leading to an r.m.s energy resolution of less than 6 % for 511 keV photons. To our knowledge such a performance as not been achieved so far.

Performance of the Annihilation Detector

Comprehensive Monte Carlo simulations have been used to study the performance of this detector arrangement.

The single-track reconstruction efficiency is close to 85 % of 4π. This corresponds approximately to the solid angle of the outer Si strip detector layer, since the efficiency of the strip detectors is close to 100 %. The annihilation vertex is reconstructed by extrapolating the (x,y,z) information derived from the Si strip detectors to their common origin. The vertex resolution is mainly limited by the extrapolation error stemming from the (unknown) curvature of the charged pion tracks in the 3 T magnetic field. In figure 6 we included the tracks for one event. Using a series of such events GEANT simulations give a radial vertex resolution of $\sigma_r = 1.5$ mm. Along the z axis, the resolution is determined by the pad pitch on the backside of the strip detectors, and is $\sigma_z \sim 3$ mm.

The solid angle for photon detection is 66 % of 4π. However, the conversion probability for a 511 keV photon ('photopeak') in a CsI crystal is only 15 %, yielding a detection efficiency of about 10 % per photon. For two collinear photons, this gives a 2-photon detection efficiency of 1.5 %. A 'golden' antihydrogen event (= 2 charged tracks and 2 back-to-back photons) has therefore a detection efficiency of about 1 %.

The high granularity of the electromagnetic calorimeter is necessary to distinguish 511 keV photons generated in antihydrogen annihilations from the random 511 keV background produced in antiproton-nucleon annihilations. The main mechanism responsible for this background is as follows: most antiproton-nucleon annihilations generate one or more neutral pions, which decay rapidly into two gammas in the 50-500 MeV energy range. These high-energy photons have a large conversion probability in the magnet coils and other material close to the central magnet bore, where they produce an electromagnetic shower with many electron-positron pairs. These positrons annihilate within a few mm radius from their production point, each giving rise to two 511 keV photons, which may then convert in one of the crystals and fake a coincidence with the antiproton annihilation. By using the high granularity of the detector, it is possible to identify true back-to-back coincidences. Using the charged vertex information, the angle between two 511 keV photons as seen from this vertex can be calculated. While antihydrogen events produce a peak at cos α = -1 (180 deg), the random background yields a flat distribution.

3.5 Outlook

The first antiproton beam from the AD for physics experiments was available early 2000. We have used this initial beam to optimize antiproton capture, demonstrate electron cooling, and confirm the ability to stack successive pulses into the Penning trap. The positron accumulator has been set up and the beam line connecting it to the main system is now active. This gives us all the ingredients to start with the first phase of the experiment. In this phase I, we will study the recombination of antiprotons and positrons as a function of plasma temperatures and densities. Different ways of bringing the two plasmas into contact will be tested, and the effect on the recombination rate and the energy distribution of antihydrogen studied. Also, for the first time, the interaction of antihydrogen with the residual gas - in particular with hydrogen atoms and molecules - will be measured. For this no attempt to capture the formed antihydrogen atoms will be made. This decision allowed us to use the maximum space in the apparatus for the detector, which enabled us to achieve the high granularity and the good vertex resolution, which are are crucial ingredients to understanding the dynamics of antihydrogen formation, as our simulations have shown.

The second phase will be designed and constructed based on the results of Phase 1. While the focus is on 2-photon laser spectroscopy of magnetically trapped antihydrogen atoms, other measurements (e.g. a measurement of the hyperfine structure using an atomic antihydrogen beam) are being explored for this program.

In order to confine the atoms once produced, the force exerted by a magnetic field gradient onto its magnetic moment may be used. Atoms in the so-called 'low field seeking' states can be trapped in a magnetic field minimum as long as the difference between their total magnetic energy at the 'edge' of the trap to the energy at the center is higher than the kinetic energy of the atoms at the center. In order to avoid transitions from the 'low field seeking states' to the 'high field seeking states' the central field value must be non-zero since otherwise spin-depolarizing Majorana transitions would occur through mixing of the different magnetic substates at zero field.

The trap configuration used to confine low-field seeking hydrogen atoms normally consists of an arrangement of coils known as Ioffe-Pritchard trap [41,51], designed to produce a magnetic minimum at the center of the trap without having a zero field location. Axial confinement is achieved through coaxial solenoids at either end of the trapping volume, which provide a barrier against axial leakage and also the non-zero field value in the center. Radial confinement is effected by superimposing a quadrupole (or higher multipole) field over the entire length of the axial well. Ioffe-Pritchard magnetic traps have been successfully used by the groups at MIT [52] and Amsterdam [53]. Typically trap depths of 1 K were achieved.

A number of open questions arise in this context, like the stability of the charged plasmas in such a magnetic field, or the achievable well depth in relation to the energy distribution of the produced antihydrogen atoms using different recombination scenarios. An active R&D program will be necessary to clarify

some of these issues before a proper design of the phase II apparatus can be attempted and has been initiated in our collaboration.

References

1. G. Lüders: Kong. Danske Vidensk. Selsk. Mat.-Fys. Medd. **28**, 1 (1957); and G. Lüders: Ann. Phys. **2**, 1 (1954)
2. W. Pauli: in: *Niels Bohr and the Development of Physics*, ed. by W. Pauli (Pergamon, New York) pp. 30–57 (1955)
3. J. S. Bell: Proc. Roy. Soc. A **231**, 479 (1955)
4. R. Jost: Helv. Phys. Acta **30**, 409 (1957) and R. Jost: *The General Theory of Quantized Fields* American Mathematical Society, Providence, Rhode Island, (1965)
5. J. J. Sakurai: *Invariance Principles and Elementary Particles* Princeton University Press, Princeton (1964) and R. F. Streater, and A. S. Wightman: *PCT, Spin & Statistics, and All That* (Benjamin, New York, 1964)
6. Particle Data Group: Phys. Lett. B**204**, 46 (1988)
7. R. S. Van Dyck: P. B. Schwinberg, and H. G. Dehmelt: Phys. Rev. Lett. **59**, 26 (1987)
8. G. Gabrielse, D. Phillips, W. Quint, H. Kalinowsky, and G. Rouleau: Phys. Rev. Lett. **74**, 3544 (1995)
9. E. Shabalin: Physics of Atomic Nuclei **57**, 1862 (1994)
10. C. M. Will: *Theory and Experiment in Gravitational Physics* Cambridge University Press, Cambridge (1981)
11. M. M. Nieto, and T. G. Goldman: Physics Reports **205**, 221 (1991)
12. F. C. Witteborn, and W. M. Fairbank: Phys. Rev. Lett. **19**, 1049 (1967)
13. R. Colella, A. W. Overhauser, and S. A. Werner: Phys. Rev. Lett. **34**, 1472 (1975)
14. R. J. Hughes: in *New and Exotic Phenomena'90*, eds. O. Fackler and J. Thranh Thanh Van, Editions Frontieres, Gif-sur-Yvettes, 1990) pp. 263–275
15. T. Goldman, R. J. Hughes, and M. M. Nieto: Phys. Lett B **171**, 217 (1986)
16. W. G. Unruh, and G. I. Opat: Am. J. Phys. **47**, 743 (1979)
17. A. Einstein: Ann. Phys. **35**, 898 (1911)
18. R. H. Dicke: in *Relativity, Groups and Topology* editors C. DeWitt and B. DeWitt, Gordon and Breach, New York (1964) pp. 163–313
19. L. I. Schiff: Am. J. Phys. **28**, 340 (1960)
20. K. Nordvedt: Phys. Rev. D **11**, 245 (1975)
21. G. Gabrielse, S. L. Rolston, L. Haarsma, and W. Kells: Phys. Lett. A**129**, 38 (1988)
22. R. Neumann, H. Poth, A. Wolf, and A. Winnacker: Z. Phys. A**313**, 253 (1984)
23. B. I. Deutch, F. M. Jacobsen, L. H. Andersen, P. Hvelplund, H. Knudsen, M. H. Holzscheiter, M. Charlton, and G. Laricchia: Phys. Scrip. T**22**, 288 (1988)
24. B. I. Deutch, L. H. Andersen, P. Hvelplund, F. M. Jacobsen, H. Knudsen, M. H. Holzscheiter, M. Charlton, and G. Laricchia: Hyperfine Interactions **44**, 271 (1988)
25. M. Charlton: Phys. Lett. A**143**, 143 (1990)
26. B. I. Deutch, M. Charlton, M. H. Holzscheiter, P. Hvelplund, L. V. Jørgensen, H. Knudsen, G. Laricchia, J. P. Merrison, and M. R. Poulsen: Hyperfine Interactions **76**, 153 (1993)
27. C. T. Munger, M. Mandelkern, J. Schultz, G. Zioulas, T. A. Armstrong, M. A. Hasan, R. A. Lewis, and G. A. Smith: *Fermilab Proposal P862* (1992)

28. H. Dehmelt, R. Van Dyck, P. Schwinberg, and G. Gabrielse: Bull. Am. Phys. Soc. **24**, 757 (1979)
29. T. Yamazaki, E. Widmann, R. S. Hayano, M. Iwasaki, S. N. Nakamura, K. Shigaki, F. J. Hartmann, H. Daniel, T. von Egidy, P. Hofmann, Y. S. Kim, and J. Eades; Nature **361**, 238 (1993)
30. Y. Ito, E. Widmann, and T. Yamazaki: Hyperfine Interactions **76**, 163 (1993)
31. G. Budker, and A. N. Skrinsky: Sov. Phys. Usp. **21**, 278 (1978)
32. H. A. Bethe, and E. E. Salpeter: *Quantum Mechanics of One- and Two-Electron Atoms*, Plenum, New York (1977)
33. M. Bell, and J. S. Bell: Part. Acc. **12**, 49 (1982)
34. A. Wolf *et al.*: Z. Phys. D**21**, 69 (1991)
35. A. Müller, and A. Wolf: Hyperfine Interactions **109**, 233 (1997)
36. U. Schramm, J. Berger, M. Grieser, D. Habs, E. Jaeschke, G. Kilgus, D. Schwalm, A. Wolf, R. Neumann, and R. Schuch: Phys. Rev. Lett. **67**; 22 (1991)
37. M. E. Glinsky, and T. M. O'Neil: Phys. Fluids B**3**, 1279 (1991)
38. M. Pajek, and R. Schuch: Hyperfine Interactions **108**, 185 (1997)
39. M. H. Holzscheiter *et al.*: Phys. At. Nucl. **57**, 1870 (1994)
40. M. H. Holzscheiter: Physica Scripta **46**, 272 (1992)
41. Y. V. Gott, M. S. Ioffe, and V. G. Tel'kovskii: Nucl. Fusion, Supplement Pt. **3**, 1045 (1962)
42. W. Thompson, and S. Hanrahan: Jour. Vac. Sci. Tech. **14**, 643 (1977)
43. J. F. Ziegler, J. P. Biersack, and U. Littmark: *The Stopping and Range of Ions in Solids*, Pergamon Press, New York (1999)
44. GEANT3: CERN Program Library Long Writeup W5013
45. D. Manuzio: Tesi di Laurea Fisica; Universitá degli Studi di Genova, Facoltá di Scienze M.F.N. (2000)
46. W. H. Barkas, W. Birnbaum, and F. M. Smith: Phys. Rev. **101**, 778 (1956)
47. G. Gabrielse, X. Fei, L. A. Orozco, S. L. Rolston, R. L. Tjoelker, T. A. Trainor, J. Haas, H. Kalinowsky, and W. Kells; Phys. Rev. A**40**, 481 (1989)
48. T. J. Murphy, and C. M. Surko: Phys. Rev. A**46**, 5696 (1992) and R. G. Greaves, M. D. Tinkle, and C. M. Surko: Phys. Plasmas **1**, 1439 (1994)
49. M. J. T. Collier, L. V. Jørgensen, Ol. Meshkov, D. P. van der Werf, and M. Charlton: in *Non-Neutral Plasmas III* (AIP Conference Proceedings 498), eds. J. J. Bollinger, R. L. Spencer, and R. C. Davidson (1999), pp. 13–18
50. F. Sauli: *Instrumentation in High Energy Physics* World Scientific (1992)
51. D. E. Pritchard: Phys. Rev. Lett. **51**, 1336 (1983)
52. J. M. Doyle, J. C. Sandberg, I. A. Yu, D. Kleppner, and T. J. Greytak: Phys Rev Lett **67**, 603 (1991)
53. I. Setija, H. Werij, O. Luiten, M. Reynolds, T. Hijmans, and J. Walraven: Phys. Rev. Lett. **70**, 2257 (1993)